Fine structure of Rydberg states. IV. Completely resolved fine structure in D, F, and G states of ^{4}He

John W. Farley and Keith B. MacAdam*
Department of Physics, University of Arizona, Tucson, Arizona 85721

William H. Wing
Department of Physics and Optical Sciences Center, University of Arizona, Tucson, Arizona 85721
(Received 15 June 1979)

The authors have made extensive new measurements in Rydberg (n = 6–11) D, F, and G states of helium. The new data represent over 1100 individual resonance scans, totalling some 2200 h of data-collection time. In order to perform such a large number of runs, data logging has been automated by interfacing a microcomputer to an apparatus previously used to make fine-structure measurements in one- and two-electron atoms. An exhaustive analysis of possible systematic line-center shifts, including blackbody radiation effects, was carried out. The root-mean-square one-standard-deviation experimental uncertainty is 294 kHz for our 67 measurements. The large quantity of new measurements has allowed us to perform a global least-squares fit to all existing state-resolved data in D, F, and G states. The complete structure of the D, F, and G manifolds is now known for $n \geq 6$ to a precision of a few megahertz or better. Current theoretical calculations for a typical (30-GHz) interval differ from the measurements by 6×10^{-8} a.u., or over 1000 experimental standard deviations.

I. INTRODUCTION

Two general types of fine structure can be distinguished in atomic and molecular systems. The first is *relativistic fine structure*, in which we include spin-spin, spin-orbit, and quantum-electrodynamic contributions. The second is *electrostatic fine structure*. This term covers inner-electron screening, electron exchange, and core-polarization effects, which occur in all systems except hydrogenlike atoms. In several previous publications[1-6] we reported microwave-optical (MO) resonance[3] measurements of fine-structure (fs) splittings in highly excited or Rydberg states of ^{4}He. In Ref. 4 (I, hereinafter) the method was summarized and the apparatus described. Measurements of $n=6$ and 7, D to F transitions were reported. In Ref. 5 (referred to as II) results in $n=8$, 9, and 16–18 were given, and semiempirical formulas useful for fitting Rydberg series data were discussed in detail. Reference 6 (referred to as III) describes two-quantum resonances observed with an improved apparatus and reports results for $n=6$, 7, 9–12, and 16, including the first measurements of fs in G states ($L=4$).

Certain other measurements have been performed recently. Astner *et al.*[7] have reported beam-foil quantum-beat measurements of the $n\,^3D_1$-$n\,^3D_2$ ($n=3$–8) intervals in ^{4}He with uncertainties of 0.6–3 MHz. Their result in $n=7$ differed by 6 MHz from our own (I). The calculational method described by Van den Eynde *et al.*[8] was extended by Tam[9] to ^3D states. Tam's result underscored the disagreement in $n=7$. We have re-examined these results and have concluded (Sec. V) that a transition was misidentified in I.

Intervals between ^1D or ^3D and high-L states for $n=7$–10, $L=3$–7 also have been reported by Beyer and Kollath,[10] who used the magnetic field anticrossing technique with a small auxiliary electric field. The uncertainties of their measurements are much larger than those routinely obtained in our MO resonance work, typically by two orders of magnitude. Nevertheless, their data extend observations of helium electrostatic fs to $L>4$; only one such transition had ever previously been reported.[1,2]

Rosenbluh *et al.*[11] used a CO_2 laser to measure the $7\,^1S_0$-$9\,^1P_1$ interval by motional-Stark-effect spectroscopy. The motional electric field mixed levels of different L and laser-driven transitions $7\,^1S$-$9L$ ($L=2, 4, 6, 8$) were observed.[12] These are similar to the "forest" of microwave-driven transitions reported in our earlier work at nonzero magnetic field.[2,3]

Since publishing III we have completed an extensive measurement program that has approximately doubled the total number of high-resolution measurements of ^{4}He D-F-G fs intervals. This paper presents the results. We describe briefly the automation of our microwave-optical resonance apparatus, report an extensive search for systematic errors which was made possible by automatic control, and describe in detail the new measurements in $n=6$ to 11 D, F, and G states. Sufficient data are now available in D, F, and G states that a reliable semiempirical formula for all the intervals involved, including both relativistic and elec-

trostatic splittings, can be given. Experimentally, D, F, and G Rydberg-state fine structure in ^{4}He is now a closed problem, in our opinion. We feel that there is no need for any further measurements for $n>6$ whose uncertainties much exceed 1 MHz.

II. APPARATUS MODIFICATIONS

The apparatus described in I–III was interfaced to an IMSAI 8080 "personal" microcomputer. Details will be given in a separate publication.[13] In brief, the computer controls (i) both the low-frequency reference source and a programmable microwave oscillator in the phase-locked microwave frequency chain; (ii) the current and voltage of the electron gun used to excite atoms to the states of interest; (iii) the helium pressure, by stepping-motor control of a leak valve; (iv) the microwave power, by biasing a PIN diode attenuator or by stepping-motor control of a waveguide vane attenuator; (v) an integrating digital voltmeter that measures the output of a lock-in amplifier; and (vi) an analog-to-digital (A/D) converter to measure experimental parameters. The experiment is operated by a BASIC -language program, which interrogates the experimenter for parameter settings, frequency ranges, integration times, etc. A sequence of resonance runs is then performed without human intervention, and the results are formatted and punched on paper tape at the conclusion of each run. The automation of this apparatus eliminated the tedium of manual control, made possible very long experimental runs, and facilitated extrapolation out of systematic shifts by taking repeated runs under varied operating conditions.

Both one- and two-quantum resonances were studied in the work reported here. In several cases, the transition energy corresponds to the difference of the frequencies of two oscillators, whereas more commonly the sum provides the interval measurement. The oscillators and nominal power levels used are listed in Table I.

III. OBSERVATION OF INVERTED RESONANCES

An interesting effect which appeared during the course of the work is shown in Fig. 1. A scan of the $10\,^3D$-$10F$ transition group shows four upright peaks, composed of six incompletely resolved resonances, and two just-resolved inverted peaks, composed of one resonance each. The upright resonances connect to the "triplet" F states, while the inverted resonances connect to the "singlet" F

TABLE I. Microwave oscillators and power levels. Oscillators: A, OKI 24V11 klystron; B, Hewlett-Packard 8620C programmable sweep oscillator; C, Varian VA290C klystron; D, Varian BL814 klystron.

One-photon microwave transition groups

Microwave transition group	Optical transition monitored (nm)	Nominal microwave interval (GHz)	Microwave source	Nominal microwave power level (μW) [a]
$6F$ -$6G$	$5\,^1D$-$2\,^1P$(439)	8.8	C	10
$8\,^3D$-$8F$	$8\,^3D$-$2\,^3P$(363)	30.5	C [b]	1
$9\,^1D$-$9F$	$9\,^1D$-$2\,^1P$(387)	14.9	B	2
$9\,^3D$-$9F$	$9\,^3D$-$2\,^3P$(359)	21.5	A	20
$10\,^3D$-$10F$	$10\,^3D$-$2\,^3P$(355)	15.8	B	1
$11\,^3D$-$11F$	$11\,^3D$-$2\,^3P$(353)	11.9	D	0.3

Two-photon microwave transition groups

Microwave transition group	Optical transition monitored (nm)	Nominal microwave interval (GHz)	Microwave source 1 (ν_1)	Microwave source 2 (ν_2)	Nominal microwave power level (μW) [a]
$7\,^3D$- $7G$	$7\,^3D$-$2\,^3P$(371)	50.8	A(25.4)	A(25.4)	100
$8\,^1D$- $8G$	$8\,^1D$-$2\,^1P$(393)	25.1	B(12.6) [c]	B(12.6) [c]	20
$8\,^3D$- $8G$	$8\,^3D$-$2\,^3P$(363)	34.4	B(12.4)	A(22.0)	30
$9\,^3D$- $9G$	$9\,^3D$-$2\,^3P$(359)	24.3	B(12.2) [c]	B(12.2) [c]	25
$10\,^1D$-$10G$	$10\,^1D$-$2\,^1P$(383)	12.9	A(22.0)	C (9.1)	10
$11\,^1D$-$11G$	$11\,^1D$-$2\,^1P$(381)	9.7	A(26.0)	B(16.3)	15
$11\,^3D$-$11G$	$11\,^3D$-$2\,^3P$(353)	13.4	A(22.2)	C (8.8)	10

[a] Flux through an area of roughly 10 cm^2.
[b] Frequency-tripled in Narda V517B R-band mixer.
[c] Amplified by Alfred 563A X-band amplifier.

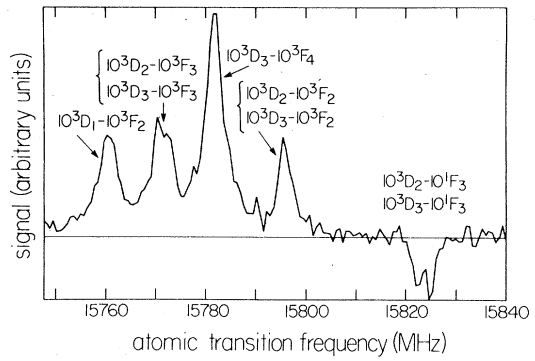

FIG. 1. Power-broadened scan of transition group 10^3D-$10F$. Resonances involving ^1F states are inverted, while resonances involving ^3F states are normal. Electron bombarding voltage is 31 V, beam current is 1 mA, helium pressure is 5×10^{-4} Torr (corrected Bayard-Alpert gauge reading).

states. The inversion arises when the F state is more populated than the D state. This effect is not due simply to electron excitation or radiative cascade from higher states, because it depends on the helium pressure. Instead, it probably results from collisional excitation transfer proceeding from more copiously excited S, P, and D "source" states. The saturated intensities suggest that the $10\,^1F_3$ state is most strongly populated, the $10\,^3F_2$ and $10\,^3F_3$ states are moderately and about equally populated, and the $10\,^3F_4$ state is much less populated than the others. At the 31-eV bombarding energy, both singlet and triplet low-L source states are excited. Related effects were reported in I. Further study along these lines could yield collisional excitation transfer cross sections, resolved with respect to fine structure.

IV. DATA ANALYSIS

A. Search for systematic errors using $9\,^1D_2$-$9\,^{1,3}F_3$ resonances

The $9\,^1D_2$-$9\,^1F_3$ and $9\,^1D_2$-$9\,^3F_3$ resonances were chosen for a series of 152 resonance runs under different conditions in a search for systematic errors (Table II). As in our previous work, the line centers were obtained from the raw data by computer fits using a multidimensional nonlinear least-squares variant of the Newton-Raphson method. The line shape incorporated into the fitting program is the sum of a Lorentzian resonance and a linear background. Adding a variable dispersion component to the Lorentzian did not improve the fit. The line centers returned by the fitting program were then least-squares analyzed for shifts with operating conditions. The functional dependence of the hypothetical center shifts on operating conditions is expressed in Eq. (1):

$$\nu-\nu_0=a_1R+a_2P+a_3IP(V-24.6)^{1/2}+a_4V^2+a_5I^2/V+a_6IP^2(V-24.6)^{1/2}. \quad (1)$$

Here ν is the measured line center, ν_0 is the extrapolated "true" line center, R is the microwave power, P is the helium pressure, I is the electron beam current, and V is the electron bombarding voltage. The adjustable coefficients a_1 through a_6 represent the following effects: a_1, an rf Stark shift, i.e., a center shift proportional to rf power; a_2, a shift linear in the helium pressure; a_3, a shift proportional to the rate of collisions of the excited atoms with helium ions; a_4, a shift quadratic in the electron beam voltage, as would result from a quadratic Stark effect produced by charging of surfaces in the experimental module; a_5, a Stark shift quadratic in the estimated electron space-charge electric field; and a_6, a quadratic Stark shift from the ion space-charge fields. The two terms associated with the coefficients a_3 and a_6 are proportional to the density of helium ions. We have roughly modeled the energy dependence of the helium ionization cross section by the square root of the electron bombarding voltage above threshold. The adjusted coefficients are given in Table III.

All the corrections listed in Table III were applied to the $9\,^1D_2$-$9\,^{1,3}F_3$ data. Net line-center shifts were less than one standard deviation (SD). The most significant coefficients proved to be the rf Stark coefficient a_1 and the surface-charging Stark coefficient a_4. However, the latter effect appeared with an unexpected positive sign. Since static Stark shifts of the D-F transition frequencies are negative, this would indicate that the surface-charging fields decrease with increasing bombarding voltage. This is contrary both to expectation and to our previous experience with grossly contaminated modules. The surface-charging term may be serving as a proxy for another effect, not incorporated into Eq. (1).

For other single-quantum transitions, for which fewer runs were taken, the shift analysis produced no coefficients significant at the two-SD level. In

TABLE II. Ranges of experimental parameters covered in search for systematic effects in the $9\,^1D_2$-$9\,^{1,3}F_3$ resonances.

Parameter	Range $9\,^1D_2$-$9\,^1F_3$	Range $9\,^1D_2$-$9\,^3F_3$
Electron gun voltage (V)	29 – 59	29 – 59
Electron current (μA)	50 –500	40 –500
rf power (μW)	0.11– 16.8	0.72– 14.0
Pressure (mTorr)	0.25– 6.1	0.56– 2.4

TABLE III. Systematic effects in $9\,^1D_2$-$9\,^{1,3}F_3$ resonances. Only the rf Stark shift is significant at the two-SD level.

Effect	Symbol	Value $9\,^1D_2$-$9\,^1F_3$	Value $9\,^1D_2$-$9\,^3F_3$
rf Stark shift (MHz/μW) [a]	a_1	-0.013 ± 0.004	-0.019 ± 0.009
Linear pressure shift (MHz/Torr)	a_2	22 ± 112	66 ± 253
Ion collision shift (MHz/μA/Torr/V$^{1/2}$)	a_3	-0.159 ± 0.151	0.30 ± 0.49
Quadratic Stark shift from surface charging (MHz/V^2)	a_4	$(3.84 \pm 1.57) \times 10^{-5}$	$(4.0 \pm 2.2) \times 10^{-5}$
Quadratic Stark shift from electron space charge (MHz V/μA^2)	a_5	$(1.9 \pm 1.2) \times 10^{-5}$	$(-1.4 \pm 1.7) \times 10^{-5}$
Quadratic Stark shift from ion space charge (MHz/μA/Torr^2/V$^{1/2}$)	a_6	0.80 ± 0.86	-0.90 ± 0.53

[a] Uncertain by a scale factor of as much as 2 representing calibration errors in microwave power measurement and transmission losses in waveguide.

view of this and of the marginal significance and uncertain interpretation of the $9\,^1D_2$-$9\,^{1,3}F_3$ effects, we did not apply corrections to the other single-quantum resonances, but instead simply averaged all runs for a given transition.

B. rf Stark corrections to two-quantum resonances

The power levels of typically 10–100 mW used for two-quantum resonances produce significant rf Stark shifts. We corrected for this in all our reported results by extrapolating the apparent resonance centers to zero rf power. Figure 2 shows two scans at different microwave power levels over the pair of resonances $7\,^3D_2$-$7\,^3G_3$ and $7\,^3D_3$-$7\,^3G_3$. The resonances scanned at higher microwave power are shifted to higher frequency by approximately 0.5 MHz. Other potential corrections were not significant, and therefore were not applied.

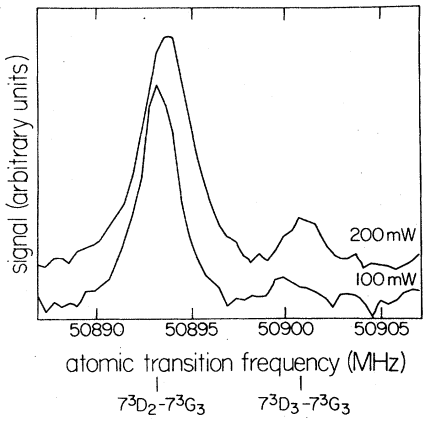

FIG. 2. Two scans of the $7\,^3D_2$-$7\,^3G_3$ and $7\,^3D_3$-$7\,^3G_3$ resonances at two different microwave power levels. The resonance center shifts with the microwave power level because of the rf Stark effect.

C. Blackbody-radiation effects and residual static Stark shift corrections

There remains the possibility of a systematic shift caused by perturbations which did not vary significantly from run to run. Such a shift would be present always and would not be detected by our extrapolation procedure. The high polarizability of Rydberg atoms makes it probable that such a shift, if present, was a Stark shift. We have considered two such possibilities; a dynamic Stark shift from blackbody radiation and a static Stark shift.

Blackbody radiation may, under some circumstances, have non-negligible effects on Rydberg atoms.[14] We have calculated the second-order shift of the energy levels studied here, summed over intermediate states, and integrated over the blackbody spectrum. Details of this calculation will be submitted separately.[15] The experimental shifts were calculated as an appropriately weighted average of the shifts caused by the 1400 °K cathode and the 300 °K module walls. The largest transition frequency shifts, for the $11D$-$11G$ transitions, were less than 2 kHz and are therefore negligible.

Next, we have considered the possibility of a Stark shift caused by a static electric field which was substantially constant from run to run. Such a field could conceivably arise in a number of ways. For example, if the helium ion density were a weakly varying function of the electron beam voltage, which would be the case if the ions were trapped, then the microscopic and macroscopic ionic electric field shifts would not extrapolate away linearly as operating conditions were reduced to zero. Alternatively, the electrostatic shielding and electron space charge in the module may have neutralized all but a relatively constant residual electric field caused by, for example,

electrode surface properties or contact potential differences. This shift might also represent an effective value of shifts which did vary from run to run, at a level below the sensitivity of our shift analysis procedure, as applied to a small run group.

We have estimated the magnitude of the effective residual electric field in two ways. First, we studied the excess linewidth of the raw data used to obtain the $16\,^1P_1$-$16\,^1D_2$ results reported in III. We extrapolated the resonance width to zero microwave power and subtracted out (a) the Zeeman broadening caused by an estimated 50 ± 50 mG residual magnetic field of random direction, and (b) the calculated rate of transition to other levels induced by blackbody radiation, integrated over the blackbody spectrum. Transit-time and pressure broadening were negligible. There remained an excess linewidth of 0.49 ± 0.29 MHz over the 0.72 MHz natural width expected on the basis of the lifetime calculations of Gabriel and Heddle,[16] scaled by n^3. We attributed the excess to a residual electric field, which would shift different $|M_L|$ levels differently and hence broaden the line. We calculated the polarizability $\alpha(n, L, S, |M_L|)$ in second order for each $|M_L|$ separately, using hydrogenic matrix elements.[17] Energy-level splittings were based on a combination of polarization theory[18] and our own data. We assumed equally populated M_L sublevels to calculate the net Stark broadening coefficient. The resulting estimate of the electric field in the experimental module was $\epsilon = 0.20 \pm 0.06$ V/cm.

The second estimate of the residual electric field utilized the global computer fit to all the resonance-center data (Sec. VI C), which optimized parameters in an empirical formula for the atomic energy levels. We added a Stark shift term $\frac{1}{2}\alpha(n, L, S)\epsilon^2$ to the fit, treating ϵ^2 as an adjustable parameter common to all levels. The polarizability $\alpha(n, L, S)$ was the average of the $\alpha(n, L, S, |M_L|)$ polarizabilities as calculated above.

The global fit returned a positive ϵ^2, which suggested that the effect was real. The estimate of the electric field, $\epsilon = 0.10 \pm 0.10$ V/cm, is compatible with the estimate obtained above, which is reassuring in view of the widely divergent estimation methods used.

We took the 0.20 ± 0.06 V/cm value obtained from linewidth analysis as our best estimate of the residual electric field because it is less model dependent. The indicated fractional uncertainty in ϵ^2 is 60%. We used this value and its uncertainty to adjust the resonance centers and to enlarge their SD's.

The resulting line-center corrections increase very rapidly with n and L, ranging from a negligible 4 kHz at $n = 7$ to 600 kHz for the $11D$-$11G$ transitions. The correction was less than one *unenlarged* SD for 50 of the 67 new measurements and between one and two unenlarged SD for the remaining 17 new measurements. Hence this correction, although insignificant for a single transition, was marginally significant for the ensemble of measurements.

We have applied the correction to our earlier measurements[1,4-6] also, since they were taken using the same apparatus. The experimental uncertainties of both new and old data were enlarged by adding the uncertainty in the static Stark shift correction in quadrature with the uncorrected uncertainty in the transition frequency. The mean fractional increase in the uncertainty was 36%.

D. Other systematic effects

In several cases the experimental uncertainties obtained by the above procedure were excessively small. In these cases, we believe that the limit on accuracy is set by undetermined residual systematic effects. The exhaustive analysis of the $9\,^1D_2$-$9\,^{1,3}F_3$ data (Sec. IV A above) suggests the value 50 kHz for these effects. Consequently, this is the smallest experimental uncertainty which we consider realistic, and we have assigned experimental uncertainties of 50 kHz in these cases.

V. NEW RESULTS

The manifold of individual D, F, and G energy levels for a typical principal quantum number $n \geq 5$ is shown in Fig. 3. New one- and two-quantum transition frequency measurements are listed in Table IV. Each entry represents several runs, with corrections made as described above. The new results represent over 1100 separate resonance scans, totaling some 2200 hours of data collection time. These data provide new relativistic fs intervals for three D states ($n = 8$, 9, and 11), four F states ($n = 8$, 9, 10, and 11), and four G states ($n = 7$, 8, 9, and 11), as well as new electrostatic intervals among most of them. The accuracy is similar to that of our previous work. Over the set of new measurements, the rms one-SD uncertainty is 294 kHz.

Table IV also lists our own *previous* measurements (corrected as discussed in Sec. IV C) and those of other workers. We have included all experimental data in D, F, and G states which resolve individual fine-structure levels. Measurements of classical-spectroscopic accuracy and nearly all anticrossing measurements have therefore been excluded. For comparison, we have also listed in Table IV the best theoretical results. The

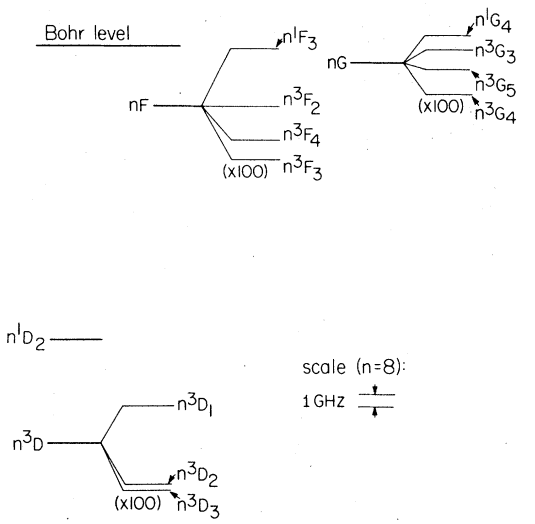

FIG. 3. Helium D-F-G energy levels (energy scale of sublevel detail expanded by a factor of 100). In F states and states of higher L, the spin-orbit interaction mixes the ${}^1L_{J=L}$ and ${}^3L_{J=L}$ states and depresses the ${}^3L_{J=L}$ below the ${}^3L_{J=L+1}$. The singlet and triplet designations for these $J=L$ states are conventional, not exact. The energy of the Bohr level, $E=-R_{\mathrm{He}}c/n^2$, is shown for reference.

compilation of theoretical calculations is not exhaustive. The experimental data constitute the input data set for a global least-squares fit, discussed in Sec. VI C, whose results are also shown in Table IV.

The frequency intervals in Table IV are grouped according to the change in the angular momentum; 0, 1, or 2. Within each group, term sequences (sequences of transitions within which only n varies) are ordered by the energy of the first state involved in the transition. The lower-energy state in a transition is listed first.

There is one case in which a discrepancy has forced a reexamination of an earlier datum. As mentioned in Sec. I, the relativistic fs interval $7\,{}^3D_1$-$7\,{}^3D_2$ measured by Astner[7] using the beam-foil quantum-beat technique is inconsistent with the result reported in I. We have therefore reexamined the raw data for the $7\,{}^3D$-$7F$ transitions. We conclude that the strong resonance at 45 136 MHz, which we previously identified as the $7\,{}^3D_3$-$7\,{}^3F_2$ resonance, is really the $7\,{}^3D_2$-$7\,{}^3F_2$ resonance. The very weak resonance we reported at 45 130 MHz, observed once with poor signal-to-noise ratio, we now attribute to a statistical fluctuation. We have, moreover, enlarged the experimental uncertainties by 900 kHz for all the $7\,{}^3D$-$7F$ data, in view of the systematic shifts reported in I but not extrapolated away. The $7\,{}^3D$-$7F$ data are now in agreement with the beam-foil measurements, and also with the $7\,{}^3D$-$7G$ data reported in this work.

VI. DISCUSSION

A. Comparison with other high-precision results

Only five earlier precise experimental results, all from our group, are available for direct comparison with the new measurements; they are listed in Table IV. Comparing the differences of the new and old measurements (after corrections) with their quadratically combined SD's, we find that measurements of three transitions agree within one combined SD, and four of five agree within two combined SD. The new and old $9\,{}^3D_2$-$9\,{}^1F_3$ measurements differ by 2.6 combined SD. The new measurements are all slightly lower than the old, with a mean difference of 294 kHz or 15 ppm of the mean frequency. On the whole, the agreement with previous measurements is excellent. It is regrettable that there are so few previous measurements for comparison; we have none at all for comparison with our two-photon measurements.

Theoretical estimates by Chang and Poe,[19,20] based on Brueckner-Goldstone perturbation theory, are listed for D-F transitions. The theoretical estimates are all lower than the experimental values, typically by 1.3%. The magnitude of the disagreement is 100–400 MHz, depending on the frequency. Experimental accuracy is thus two-and-a-half to three orders of magnitude greater than that of the theory. Chang and Poe express their results as a power series in the principal quantum number n:

$$E=A/n^3+B/n^5+C/n^7. \tag{2}$$

E represents the displacement from the Bohr level of a singly excited helium atom exhibiting perfect screening. The theory is currently so inaccurate that only the first term in the expansion is really justified. Only when the calculation of the leading coefficient is improved will theoretical calculations of the higher-order terms become meaningful.

B. Test of internal consistency in data set

As mentioned in Sec. VI A, there are only a few cases where we have remeasured a transition. There are, therefore, few opportunities for direct comparison between new and old transition frequencies. We have, however, checked for internal consistency among the transition data corresponding to a single value of the principal quantum number n by adjusting the energies of the twelve levels that make up the nD, nF, and nG manifolds in order to obtain a best fit of all the

TABLE IV. Fine-structure intervals in D, F, and G states of ^{4}He. All state-resolved experimental results and selected theoretical results are included. Frequencies listed without uncertainties are theoretical estimates.

Interval	Frequency (MHz)	Global fit (MHz)	Fit − expt. / expt. uncert.	Method [s]	Reference [t]
$3\,^3D_3$- $3\,^3D_2$	75.97 ± 0.23	75.258 ± 0.388	−3.094	LC	Tam [a] (E)
	72.5 ± 0.5		5.516	LC	Descoubes [b] (E)
	71 ± 2		2.129	BF	Berry [c] (E)
	85.8				Tam [d] (T)
	83.8				Bessis [e] (T)
	69.6				Chang [f] (T)
	92.7				Bethe [g] (T)
$4\,^3D_3$- $4\,^3D_2$	36.15 ± 0.24	36.363 ± 0.360	0.888	LC	Tam [a] (E)
	35.8 ± 0.4		1.408	LC	Descoubes [b] (E)
	40 ± 5		−0.727	BF	Berry [c] (E)
	41.8				Tam [d] (T)
	41.1				Bessis [e] (T)
	31.5				Chang [f] (T)
	39.1				Bethe [g] (T)
$5\,^3D_3$- $5\,^3D_2$	20.3 ± 0.3	19.543 ± 0.180	−2.522	LC	Descoubes [b] (E)
	19 ± 3		0.181	BF	Berry [c] (E)
	22.5				Tam [d] (T)
	24.0				Bessis [e] (T)
	16				Chang [f] (T)
	20.0				Bethe [g] (T)
$6\,^3D_3$- $6\,^3D_2$	12.2 ± 0.3	11.575 ± 0.134	−2.084	LC	Descoubes [b] (E)
	13.35				Tam [d] (T)
	15.1				Bessis [e] (T)
	9.6				Chang [f] (T)
	11.6				Bethe [g] (T)
$7\,^3D_3$- $7\,^3D_2$	7.3 ± 0.3	7.384 ± 0.106	0.281	LC	Descoubes [b] (E)
	8.62				Tam [d] (T)
	10.0				Bessis [e] (T)
	6.3				Chang [f] (T)
	7.3				Bethe [g] (T)
$8\,^3D_3$- $8\,^3D_2$	3.75	4.987 ± 0.083			Chang [f] (T)
$9\,^3D_3$- $9\,^3D_2$	2.65	3.521 ± 0.065			Chang [f] (T)
$10\,^3D_3$-$10\,^3D_2$	1.94	2.576 ± 0.051			Chang [f] (T)
$11\,^3D_3$-$11\,^3D_2$	1.46	1.941 ± 0.041			Chang [f] (T)
$12\,^3D_3$-$12\,^3D_2$	1.13	1.498 ± 0.033			Chang [f] (T)
$20\,^3D_3$-$20\,^3D_2$	0.25	0.326 ± 0.008			Chang [f] (T)
$3\,^3D_3$- $3\,^3D_1$	1400.67 ± 0.29	1400.759 ± 0.531	0.306	LC	Tam [a] (E)
	1392				Chang [f] (T)
	1390				Bethe [g] (T)
$4\,^3D_3$- $4\,^3D_1$	591.25 ± 0.14	591.194 ± 0.261	−0.398	LC	Tam [a] (E)
	586				Chang [f] (T)
	587				Bethe [g] (T)
$5\,^3D_3$- $5\,^3D_1$	303 ± 6	302.881 ± 0.216	−0.020	LC	Descoubes [b] (E)
	331 ± 58		−0.485	AC	Beyer [i] (E)
	300				Chang [f] (T)
$6\,^3D_3$- $6\,^3D_1$	270 ± 30	175.358 ± 0.203	−3.155	LC	Descoubes [b] (E)
	194 ± 70		−0.266	AC	Beyer [i] (E)
	174				Chang [f] (T)
$7\,^3D_3$- $7\,^3D_1$	142 ± 38	110.464 ± 0.166	−0.830	AC	Beyer [i] (E)
	109				Chang [f] (T)
$8\,^3D_3$- $8\,^3D_1$	73.24	74.018 ± 0.130			Chang [f] (T)
$9\,^3D_3$- $9\,^3D_1$	51.44	51.994 ± 0.101			Chang [f] (T)
$10\,^3D_3$-$10\,^3D_1$	37.50	37.908 ± 0.079			Chang [f] (T)
$11\,^3D_3$-$11\,^3D_1$	28.17	28.483 ± 0.063			Chang [f] (T)
$12\,^3D_3$-$12\,^3D_1$	21.70	21.941 ± 0.050			Chang [f] (T)
$20\,^3D_3$-$20\,^3D_1$	4.69	4.740 ± 0.012			Chang [f] (T)
$3\,^3D_2$- $3\,^3D_1$	1327.2 ± 1.1	1325.500 ± 0.639	−1.545	LC	Kaul [j] (E)
	1323.6 ± 2.3		0.826	BF	Astner [k] (E)

TABLE IV. *(Continued)*

Interval	Frequency (MHz)	Global fit (MHz)	Fit − expt. / expt. uncert.	Method[s]	Reference[t]
$3\,^3D_2$-$3\,^3D_1$	1 349 ±25		−0.940	BF	Berry[c] (E)
	1 359 ±30		−1.117	LC	Brochard[l] (E)
	1 322				Chang[f] (T)
	1 328				Tam[d] (T)
	1 325				Bessis[e] (T)
	1 297				Bethe[g] (T)
	1 346				Parish[h] (T)
$4\,^3D_2$- $4\,^3D_1$	553.0 ± 0.7	554.831 ± 0.430	2.616	BF	Astner[k] (E)
	536 ±30		0.628	BF	Berry[c] (E)
	561 ±30		−0.206	LC	Brochard[l] (E)
	555				Chang[f] (T)
	558.3				Tam[d] (T)
	557				Bessis[e] (T)
	548				Bethe[g] (T)
	573				Parish[h] (T)
$5\,^3D_2$- $5\,^3D_1$	284.1 ± 0.6	283.338 ± 0.223	−1.271	BF	Astner[k] (E)
	282 ± 2		0.669	LC	Dily[m] (E)
	290 ±20		−0.333	BF	Berry[c] (E)
	284				Chang[f] (T)
	285.6				Tam[d] (T)
	294				Parish[h] (T)
$6\,^3D_2$- $6\,^3D_1$	165.3 ± 1.0	163.783 ± 0.164	−1.517	BF	Astner[k] (T)
	165.7 ± 3.0		−0.639	LC	Dily[m] (E)
	150 ±20		0.689	BF	Berry[c] (E)
	164				Chang[f] (T)
	165.3				Tam[d] (T)
	171				Parish[h] (T)
$7\,^3D_2$- $7\,^3D_1$	101.6 ± 1.1	103.080 ± 0.129	1.345	BF	Astner[k] (E)
	92 ±15		0.739	BF	Berry[c] (E)
	103				Chang[f] (T)
	104.0				Tam[d] (T)
	108				Parish[h] (T)
$8\,^3D_2$- $8\,^3D_1$	69 ± 3	69.032 ± 0.101	0.010	BF	Astner[k] (E)
	69.18				Chang[f] (T)
	69.7				Tam[d] (T)
	72				Parish[h] (T)
$3\,^3D_2$- $3\,^1D_2$	102 020.58	100 313 ±694			Chang[f] (T)
$4\,^3D_2$- $4\,^1D_2$	58 853.04	58 987.1 ± 71.1			Chang[f] (T)
$5\,^3D_2$- $5\,^1D_2$	33 913.86	34 095.3 ± 10.0			Chang[f] (T)
$6\,^3D_2$- $6\,^1D_2$	20 819.87	20 946.53 ± 1.49			Chang[f] (T)
$7\,^3D_2$- $7\,^1D_2$	13 565.46	13 650.501 ± 0.201			Chang[f] (T)
$8\,^3D_2$- $8\,^1D_2$	9 285.67	9 344.144 ± 0.091			Chang[f] (T)
$9\,^3D_2$- $9\,^1D_2$	6 617.00	6 658.534 ± 0.071			Chang[f] (T)
$10\,^3D_2$-$10\,^1D_2$	4 873.56	4 903.991 ± 0.075			Chang[f] (T)
$11\,^3D_2$-$11\,^1D_2$	3 689.26	3 712.167 ± 0.083			Chang[f] (T)
$12\,^3D_2$-$12\,^1D_2$	2 857.89	2 875.547 ± 0.086			Chang[f] (T)
$20\,^3D_2$-$20\,^1D_2$	659.11	632.910 ± 0.042			Chang[f] (T)
$5\,^3F_3$- $5\,^3F_4$	20 ± 6	83.89 ± 3.89	10.649	LC	Descoubes[b] (E)
$4\,^3D_3$- $4\,^3F_3$	217 689.33	221 451.9 ± 65.2			Chang[f] (T)
$5\,^3D_3$- $5\,^3F_3$	117 227.83	118 907.53 ± 9.44			Chang[f] (T)
$6\,^3D_3$- $6\,^3F_3$	69 591.37	70 535.06 ± 1.51			Chang[f] (T)
$7\,^3D_3$- $7\,^3F_3$	45 068.707 ± 1.063	45 069.821 ± 0.223	1.048	MO	MacAdam[n] (E)
	44 475.76				Chang[f] (T)
$8\,^3D_3$- $8\,^3F_3$	30 475.536 ± 0.057	30 475.628 ± 0.071	1.627	MO	This work (E)
	30 075				Chang[f] (T)
$9\,^3D_3$- $9\,^3F_3$	21 539.723 ± 0.103	21 539.720 ± 0.067	−0.030	MO	This work (E)
	21 540.235 ± 0.500		−1.029	MO	MacAdam[o] (E)
	21 256				Chang[f] (T)
$10\,^3D_3$-$10\,^3F_3$	15 773.096 ± 0.123	15 773.131 ± 0.074	0.286	MO	This work (E)

TABLE IV. *(Continued)*

Interval	Frequency (MHz)	Global fit (MHz)	Fit − expt. / expt. uncert.	Method [s]	Reference [t]
$10\,^3D_3$-$10\,^3F_3$	15 565				Chang [f] (T)
$11\,^3D_3$-$11\,^3F_3$	11 890.056 ± 0.260	11 889.837 ± 0.080	−0.846	MO	This work (E)
	11 732				Chang [f] (T)
$12\,^3D_3$-$12\,^3F_3$	9 059.28	9 181.180 ± 0.080			Chang [f] (T)
$20\,^3D_3$-$20\,^3F_3$	1 972.96	1 999.824 ± 0.037			Chang [f] (T)
$4\,^3D_3$- $4\,^3F_4$	217 910.24	221 633.6 ± 70.5			Chang [f] (T)
$5\,^3D_3$- $5\,^3F_4$	117 323.56	118 991.4 ± 11.0			Chang [f] (T)
$6\,^3D_3$- $6\,^3F_4$	69 641.71	70 580.75 ± 2.04			Chang [f] (T)
$7\,^3D_3$- $7\,^3F_4$	45 097.083 ± 0.957	45 097.507 ± 0.400	0.443	MO	MacAdam [n] (E)
	44 506				Chang [f] (T)
$8\,^3D_3$- $8\,^3F_4$	30 493.806 ± 0.050	30 493.704 ± 0.091	−2.057	MO	This work (E)
	30 094				Chang [f] (T)
$9\,^3D_3$- $9\,^3F_4$	21 552.120 ± 0.076	21 552.187 ± 0.067	0.894	MO	This work (E)
	21 240				Chang [f] (T)
$10\,^3D_3$-$10\,^3F_4$	15 782.014 ± 0.050	15 782.101 ± 0.074	1.725	MO	This work (E)
	15 574				Chang [f] (T)
$11\,^3D_3$-$11\,^3F_4$	11 896.339 ± 0.100	11 896.510 ± 0.077	1.719	MO	This work (E)
	11 739				Chang [f] (T)
$12\,^3D_3$-$12\,^3F_4$	9 186.129 ± 0.275	9 186.281 ± 0.075	0.552	MO	MacAdam [p] (E)
	9 065				Chang [f] (T)
$20\,^3D_3$-$20\,^3F_4$	1 974.06	2 000.897 ± 0.033			Chang [f] (T)
$4\,^3D_3$- $4\,^3F_2$	218 171.80	221 899.5 ± 70.4			Chang [f] (T)
$5\,^3D_3$- $5\,^3F_2$	117 456	119 125.9 ± 10.9			Chang [f] (T)
$6\,^3D_3$- $6\,^3F_2$	69 718.25	70 658.00 ± 2.02			Chang [f] (T)
$7\,^3D_3$- $7\,^3F_2$	44 553.81	45 145.948 ± 0.400			Chang [f] (T)
$8\,^3D_3$- $8\,^3F_2$	30 126.42	30 526.064 ± 0.117			Chang [f] (T)
$9\,^3D_3$- $9\,^3F_2$	21 574.714 ± 0.879	21 574.872 ± 0.088	0.179	MO	This work (E)
	21 292				Chang [f] (T)
$10\,^3D_3$-$10\,^3F_2$	15 590.77	15 798.615 ± 0.085			Chang [f] (T)
$11\,^3D_3$-$11\,^3F_2$	11 909.410 ± 0.246	11 908.905 ± 0.082	−2.055	MO	This work (E)
	11 752				Chang [f] (T)
$12\,^3D_3$-$12\,^3F_2$	9 074.15	9 195.821 ± 0.078			Chang [f] (T)
$20\,^3D_3$-$20\,^3F_2$	1 976.13	2 002.953 ± 0.033			Chang [f] (T)
$4\,^3D_3$- $4\,^1F_3$	218 388.92	222 115.3 ± 65.4			Chang [f] (T)
$5\,^3D_3$- $5\,^1F_3$	117 600.51	119 280.69 ± 9.45			Chang [f] (T)
$6\,^3D_3$- $6\,^1F_3$	69 813.78	70 761.55 ± 1.51			Chang [f] (T)
$7\,^3D_3$- $7\,^1F_3$	45 215.097 ± 0.953	45 216.454 ± 0.223	1.423	MO	MacAdam [n] (E)
	44 619				Chang [f] (T)
$8\,^3D_3$- $8\,^1F_3$	30 575.619 ± 0.050	30 575.601 ± 0.071	−0.356	MO	This work (E)
	30 172				Chang [f] (T)
$9\,^3D_3$- $9\,^1F_3$	21 610.601 ± 0.124	21 610.601 ± 0.061	1.376	MO	This work (E)
	21 610.733 ± 0.301		0.130	MO	MacAdam [o] (E)
	21 325				Chang [f] (T)
$10\,^3D_3$-$10\,^1F_3$	15 825.586 ± 0.093	15 825.365 ± 0.067	−2.388	MO	This work (E)
	15 616				Chang [f] (T)
$11\,^3D_3$-$11\,^1F_3$	11 929.527 ± 0.147	11 929.324 ± 0.074	−1.379	MO	This work (E)
	11 771				Chang [f] (T)
$12\,^3D_3$-$12\,^1F_3$	9 088.96	9 211.737 ± 0.076			Chang [f] (T)
$20\,^3D_3$-$20\,^1F_3$	1 979.47	2 006.527 ± 0.036			Chang [f] (T)
$7\,^3D_2$- $7\,^3F_3$	45 061.535 ± 0.959	45 062.437 ± 0.218	0.941	MO	MacAdam [n] (E)
	44 470				Chang [f] (T)
$8\,^3D_2$- $8\,^3F_3$	30 470.734 ± 0.050	30 470.642 ± 0.073	−1.859	MO	This work (E)
	30 071				Chang [f] (T)
	30 068				Chang [r] (T)
$9\,^3D_2$- $9\,^3F_3$	21 535.923 ± 0.108	21 536.199 ± 0.062	2.546	MO	This work (E)
	21 536.235 ± 0.301		−0.120	MO	MacAdam [o] (E)
	21 253				Chang [f] (T)
$10\,^3D_2$-$10\,^3F_3$	15 770.824 ± 0.113	15 770.554 ± 0.067	−2.394	MO	This work (E)
	15 563				Chang [f] (T)

TABLE IV. *(Continued)*

Interval	Frequency (MHz)	Global fit (MHz)	Fit − expt. / expt. uncert.	Method	Reference [t]
$10\,^3D_2$-$10\,^3F_3$	15 561				Chang [r] (T)
$11\,^3D_2$-$11\,^3F_3$	11 888.144 ± 0.098	11 887.896 ± 0.073	−2.525	MO	This work (E)
	11 731				Chang [f] (T)
	11 730				Chang [r] (T)
$12\,^3D_2$-$12\,^3F_3$	9 180.059 ± 0.588	9 179.682 ± 0.075	−0.643	MO	MacAdam [p] (E)
	9 058				Chang [f] (T)
$7\,^3D_2$- $7\,^3F_2$	45 136.147 ± 0.966	45 138.563 ± 0.375	2.501	MO	MacAdam [n] (E)
	44 458				Chang [f] (T)
$8\,^3D_2$- $8\,^3F_2$	30 521.106 ± 0.050	30 521.078 ± 0.082	−0.564	MO	This work (E)
	30 123				Chang [f] (T)
$9\,^3D_2$- $9\,^3F_2$	21 571.364 ± 0.054	21 571.351 ± 0.063	−0.243	MO	This work (E)
	21 289				Chang [f] (T)
$10\,^3D_2$-$10\,^3F_2$	15 795.948 ± 0.066	15 796.038 ± 0.068	1.368	MO	This work (E)
	15 589				Chang [f] (T)
$11\,^3D_2$-$11\,^3F_2$	11 906.914 ± 0.098	11 906.964 ± 0.071	0.511	MO	This work (E)
	11 750				Chang [f] (T)
$12\,^3D_2$-$12\,^3F_2$	9 194.019 ± 0.438	9 194.323 ± 0.069	0.693	MO	MacAdam [p] (E)
	9 073				Chang [f] (T)
$7\,^3D_2$- $7\,^1F_3$	45 208.031 ± 0.953	45 209.069 ± 0.224	1.090	MO	MacAdam [n] (E)
	44 613				Chang [f] (T)
$8\,^3D_2$- $8\,^1F_3$	30 570.589 ± 0.128	30 570.614 ± 0.085	0.198	MO	This work (E)
	30 168				Chang [f] (T)
$9\,^3D_2$- $9\,^1F_3$	21 606.836 ± 0.112	21 607.251 ± 0.066	3.708	MO	This work (E)
	21 607.233 ± 0.102		0.175	MO	MacAdam [o] (E)
	21 322				Chang [f] (T)
$10\,^3D_2$-$10\,^1F_3$	15 822.957 ± 0.077	15 822.788 ± 0.065	−2.187	MO	This work (E)
	15 614				Chang [f] (T)
$11\,^3D_2$-$11\,^1F_3$	11 927.231 ± 0.101	11 927.383 ± 0.070	1.490	MO	This work (E)
	11 769				Chang [f] (T)
$12\,^3D_2$-$12\,^1F_3$	9 210.214 ± 0.380	9 210.239 ± 0.072	0.065	MO	MacAdam [p] (E)
	9 088				Chang [f] (T)
$7\,^3D_1$- $7\,^3F_2$	45 034.909 ± 0.968	45 035.484 ± 0.362	0.594	MO	MacAdam [n] (E)
	44 444				Chang [f] (T)
$8\,^3D_1$- $8\,^3F_2$	30 452.028 ± 0.050	30 452.046 ± 0.083	0.367	MO	This work (E)
	30 053				Chang [f] (T)
$9\,^3D_1$- $9\,^3F_2$	21 522.975 ± 0.087	21 522.878 ± 0.077	−1.105	MO	This work (E)
	21 240				Chang [f] (T)
$10\,^3D_1$-$10\,^3F_2$	15 760.670 ± 0.141	15 760.707 ± 0.081	0.261	MO	This work (E)
	15 553				Chang [f] (T)
$11\,^3D_1$-$11\,^3F_2$	11 880.415 ± 0.098	11 880.422 ± 0.080	0.069	MO	This work (E)
	11 724				Chang [f] (T)
$12\,^3D_1$-$12\,^3F_2$	9 173.879 ± 0.253	9 173.880 ± 0.076	0.004	MO	MacAdam [p] (E)
	9 052				Chang [f] (T)
$4\,^1D_2$- $4\,^3F_3$	158 809.16	162 428.4 ± 17.4			Chang [f] (T)
$5\,^1D_2$- $5\,^3F_3$	83 299.33	84 792.70 ± 1.88			Chang [f] (T)
$6\,^1D_2$- $6\,^3F_3$	49 576.861 ± 0.090	49 576.955 ± 0.166	1.044	MO	MacAdam [n] (E)
	48 763				Chang [f] (T)
$7\,^1D_2$- $7\,^3F_3$	31 412.074 ± 0.080	31 411.936 ± 0.112	−1.728	MO	Wing [q] (E)
	30 905				Chang [f] (T)
$8\,^1D_2$- $8\,^3F_3$	21 126.512 ± 0.200	21 126.498 ± 0.071	−0.073	MO	MacAdam [o] (E)
	20 785				Chang [f] (T)
$9\,^1D_2$- $9\,^3F_3$	14 877.602 ± 0.056	14 877.665 ± 0.055	1.122	MO	This work (E)
	14 636				Chang [f] (T)
$10\,^1D_2$-$10\,^3F_3$	10 866.518 ± 0.050	10 866.563 ± 0.056	0.915	MO	MacAdam [p] (E)
	10 689				Chang [f] (T)
$11\,^1D_2$-$11\,^3F_3$	8 175.668 ± 0.137	8 175.728 ± 0.057	0.441	MO	MacAdam [p] (E)
	8 042				Chang [f] (T)
$12\,^1D_2$-$12\,^3F_3$	6 200.26	6 304.135 ± 0.054			Chang [f] (T)
$20\,^1D_2$-$20\,^3F_3$	1 343.60	1 366.588 ± 0.022			Chang [f] (T)

TABLE IV. *(Continued)*

Interval	Frequency (MHz)	Global fit (MHz)	Fit − expt. / expt. uncert.	Method [s]	Reference [t]
$4\,^1D_2$- $4\,^1F_3$	159 508.75	163 091.8 ± 17.3			Chang [f] (T)
$5\,^1D_2$- $5\,^1F_3$	83 672.02	85 165.86 ± 1.83			Chang [f] (T)
$6\,^1D_2$- $6\,^1F_3$	49 803.501 ± 0.080	49 803.446 ± 0.148	−0.694	MO	MacAdam [n] (E)
	48 985				Chang [f] (T)
$7\,^1D_2$- $7\,^1F_3$	31 558.264 ± 0.100	31 558.568 ± 0.118	3.044	MO	Wing [q] (E)
	31 048				Chang [f] (T)
$8\,^1D_2$- $8\,^1F_3$	21 226.412 ± 0.200	21 226.470 ± 0.073	0.294	MO	MacAdam [o] (E)
	20 883				Chang [f] (T)
$9\,^1D_2$- $9\,^1F_3$	14 948.723 ± 0.046	14 948.717 ± 0.053	−0.138	MO	This work (E)
	14 705				Chang [f] (T)
$10\,^1D_2$-$10\,^1F_3$	10 918.890 ± 0.050	10 918.797 ± 0.053	−1.865	MO	MacAdam [p] (E)
	10 740				Chang [f] (T)
$11\,^1D_2$-$11\,^1F_3$	8 215.206 ± 0.114	8 215.215 ± 0.054	0.084	MO	MacAdam [p] (E)
	8 080				Chang [f] (T)
$12\,^1D_2$-$12\,^1F_3$	6 229.94	6 334.692 ± 0.052			Chang [f] (T)
$20\,^1D_2$-$20\,^1F_3$	1 350.12	1 373.292 ± 0.021			Chang [f] (T)
$6\,^1F_3$- $6\,^1G_4$	8 853.965 ± 0.050	8 853.979 ± 0.093	0.285	MO	This work (E)
	8 854.062 ± 0.270		−0.306	MO	MacAdam [p] (E)
$5\,^3D_3$- $5\,^3G_4$		133 877.7 ± 10.9			
$6\,^3D_3$- $6\,^3G_4$		79 541.66 ± 1.67			
$7\,^3D_3$- $7\,^3G_4$	50 841.576 ± 0.358	50 842.603 ± 0.214	2.862	MO	This work (E)
$8\,^3D_3$- $8\,^3G_4$	34 399.018 ± 0.499	34 399.856 ± 0.166	1.678	MO	This work (E)
$9\,^3D_3$- $9\,^3G_4$	24 323.214 ± 0.131	24 323.290 ± 0.112	0.583	MO	This work (E)
$10\,^3D_3$-$10\,^3G_4$	17 827.263 ± 0.692	17 816.693 ± 0.116	−0.261	MO	MacAdam [p] (E)
$11\,^3D_3$-$11\,^3G_4$	13 434.755 ± 0.584	13 433.174 ± 0.118	−2.706	MO	This work (E)
$12\,^3D_3$-$12\,^3G_4$		10 380.759 ± 0.197			
$20\,^3D_3$-$20\,^3G_4$		2 262.352 ± 0.070			
$5\,^3D_3$- $5\,^3G_5$		133 877.7 ± 10.9			
$6\,^3D_3$- $6\,^3G_5$		79 541.66 ± 1.67			
$7\,^3D_3$- $7\,^3G_5$	50 872.636 ± 0.140	50 872.617 ± 0.262	−0.132	MO	This work (E)
$8\,^3D_3$- $8\,^3G_5$	34 420.248 ± 0.264	34 420.180 ± 0.234	−0.257	MO	This work (E)
$9\,^3D_3$- $9\,^3G_5$	24 337.302 ± 0.205	24 337.669 ± 0.248	1.790	MO	This work (E)
$10\,^3D_3$-$10\,^3G_5$	17 827.263 ± 0.206	17 827.229 ± 0.238	−0.167	MO	MacAdam [p] (E)
$11\,^3D_3$-$11\,^3G_5$	13 442.542 ± 0.405	13 441.120 ± 0.219	−3.510	MO	This work (E)
$12\,^3D_3$-$12\,^3G_5$		10 380.759 ± 0.197			
$20\,^3D_3$-$20\,^3G_5$		2 262.352 ± 0.070			
$5\,^3D_3$- $5\,^3G_3$		133 956.0 ± 10.3			
$6\,^3D_3$- $6\,^3G_3$		79 586.20 ± 1.49			
$7\,^3D_3$- $7\,^3G_3$	50 899.764 ± 0.588	50 900.366 ± 0.262	1.024	MO	This work (E)
$8\,^3D_3$- $8\,^3G_3$		34 438.641 ± 0.171			
$9\,^3D_3$- $9\,^3G_3$		24 350.573 ± 0.156			
$10\,^3D_3$-$10\,^3G_3$		17 836.604 ± 0.156			
$11\,^3D_3$-$11\,^3G_3$		13 448.146 ± 0.153			
$12\,^3D_3$-$12\,^3G_3$		10 386.160 ± 0.145			
$20\,^3D_3$-$20\,^3G_3$		2 263.511 ± 0.059			
$7\,^3D_3$- $7\,^1G_4$	50 918.948 ± 0.206	50 918.864 ± 0.201	−0.408	MO	This work (E)
$8\,^3D_3$- $8\,^1G_4$	34 451.593 ± 0.461	34 451.044 ± 0.113	−1.192	MO	This work (E)
$9\,^3D_3$- $9\,^1G_4$	24 359.035 ± 0.268	24 359.289 ± 0.125	0.951	MO	This work (E)
$10\,^3D_3$-$10\,^1G_4$	17 842.728 ± 0.326	17 842.961 ± 0.139	0.711	MO	MacAdam [p] (E)
$7\,^3D_2$- $7\,^3G_4$	50 835.466 ± 0.234	50 835.218 ± 0.210	−1.056	MO	This work (E)
$8\,^3D_2$- $8\,^3G_4$	34 394.014 ± 0.447	34 394.869 ± 0.121	1.915	MO	This work (E)
$9\,^3D_2$- $9\,^3G_4$	24 319.687 ± 0.194	24 319.769 ± 0.114	0.424	MO	This work (E)
$10\,^3D_2$-$10\,^3G_4$	17 814.593 ± 0.464	17 814.116 ± 0.115	−1.028	MO	MacAdam [p] (E)
$11\,^3D_2$-$11\,^3G_4$	13 431.690 ± 0.556	13 431.233 ± 0.117	−0.821	MO	This work (E)
$7\,^3D_2$- $7\,^3G_3$	50 892.976 ± 0.180	50 892.981 ± 0.241	0.028	MO	This work (E)
$8\,^3D_2$- $8\,^3G_3$	34 433.052 ± 0.353	34 433.654 ± 0.154	1.706	MO	This work (E)
$9\,^3D_2$- $9\,^3G_3$	24 347.078 ± 0.094	24 347.052 ± 0.142	−0.282	MO	This work (E)
$10\,^3D_2$-$10\,^3G_3$	17 834.183 ± 0.356	17 834.028 ± 0.145	−0.438	MO	MacAdam [p] (E)
$11\,^3D_2$-$11\,^3G_3$	13 446.806 ± 0.664	13 446.205 ± 0.146	−0.905	MO	This work (E)

TABLE IV. *(Continued)*

Interval	Frequency (MHz)	Global fit (MHz)	Fit − expt. / expt. uncert.	Method [s]	Reference [t]
$7\,^3D_2$- $7\,^1G_4$	50 911.423 ± 0.161	50 911.480 ± 0.197	0.353	MO	This work (E)
$8\,^3D_2$- $8\,^1G_4$	34 446.363 ± 0.366	34 446.057 ± 0.117	−0.837	MO	This work (E)
$9\,^3D_2$- $9\,^1G_4$	24 355.617 ± 0.223	24 355.768 ± 0.125	0.676	MO	This work (E)
$10\,^3D_2$-$10\,^1G_4$	17 840.458 ± 0.310	17 840.384 ± 0.137	−0.239	MO	MacAdam [p] (E)
$11\,^3D_2$-$11\,^1G_4$	13 451.721 ± 0.774	13 450.982 ± 0.141	−0.954	MO	This work (E)
$7\,^3D_1$- $7\,^3G_3$	50 790.047 ± 0.177	50 789.902 ± 0.241	−0.816	MO	This work (E)
$8\,^3D_1$- $8\,^3G_3$	34 364.594 ± 0.294	34 364.622 ± 0.162	0.096	MO	This work (E)
$9\,^3D_1$- $9\,^3G_3$	24 298.383 ± 0.160	24 298.580 ± 0.150	1.226	MO	This work (E)
$10\,^3D_1$-$10\,^3G_3$	17 798.863 ± 0.338	17 798.696 ± 0.150	−0.494	MO	MacAdam [p] (E)
$11\,^3D_1$-$11\,^3G_3$	13 420.854 ± 0.428	13 419.663 ± 0.149	−2.780	MO	This work (E)
$5\,^1D_2$- $5\,^3G_4$		99 684.13 ± 4.27			
$6\,^1D_2$- $6\,^3G_4$		58 536.686 ± 0.633			
$7\,^1D_2$- $7\,^3G_4$	37 184.738 ± 0.050	37 184.717 ± 0.092	−0.417	MO	MacAdam [p] (E)
$8\,^1D_2$- $8\,^3G_4$	25 050.702 ± 0.088	25 050.729 ± 0.088	0.261	MO	This work (E)
$9\,^1D_2$- $9\,^3G_4$	17 661.220 ± 0.077	17 661.235 ± 0.100	0.195	MO	MacAdam [p] (E)
$10\,^1D_2$-$10\,^3G_4$	12 911.252 ± 0.271	12 910.125 ± 0.100	−4.162	MO	This work (E)
$11\,^1D_2$-$11\,^3G_4$	9 718.443 ± 0.366	9 719.066 ± 0.094	1.700	MO	This work (E)
$12\,^1D_2$-$12\,^3G_4$		7 497.575 ± 0.085			
$20\,^1D_2$-$20\,^3G_4$		1 627.778 ± 0.031			
$5\,^1D_2$- $5\,^1G_4$		99 891.73 ± 2.42			
$6\,^1D_2$- $6\,^1G_4$		58 657.424 ± 0.175			
$7\,^1D_2$- $7\,^1G_4$	37 261.027 ± 0.050	37 260.979 ± 0.088	−0.967	MO	MacAdam [p] (E)
$8\,^1D_2$- $8\,^1G_4$	25 101.803 ± 0.075	25 101.913 ± 0.081	1.474	MO	This work (E)
$9\,^1D_2$- $9\,^1G_4$	17 697.196 ± 0.088	17 697.234 ± 0.112	0.435	MO	MacAdam [p] (E)
$10\,^1D_2$-$10\,^1G_4$	12 937.121 ± 0.282	12 936.393 ± 0.126	−2.582	MO	This work (E)
$11\,^1D_2$-$11\,^1G_4$	9 739.380 ± 0.537	9 738.815 ± 0.124	−1.053	MO	This work (E)
$12\,^1D_2$-$12\,^1G_4$		7 512.795 ± 0.116			
$20\,^1D_2$-$20\,^1G_4$		1 613.072 ± 0.042			

[a] Tam, Ref. 21.
[b] Descoubes, Ref. 22.
[c] Berry, Ref. 23.
[d] Tam, Ref. 9.
[e] Bessis, Ref. 24.
[f] Chang, Ref. 19.
[g] Bethe, Ref. 17.
[h] Parish, Ref. 25.
[i] Beyer, Ref. 26.
[j] Kaul, Ref. 27.
[k] Astner, Ref. 7.
[l] Brochard, Ref. 28.
[m] Dily, Ref. 29.
[n] MacAdam and Wing, Ref. 4.
[o] MacAdam and Wing, Ref. 5.
[p] MacAdam and Wing, Ref. 6.
[q] Wing and Lamb, Ref. 1.
[r] Chang, Ref. 20.
[s] LC, level-crossing; BF, beam-foil quantum beats; AC, magnetic field anticrossing; MO, microwave-optical resonance.
[t] E, experimental; T, theoretical.

measured transition frequencies for that n listed in Table IV. Each datum was weighted statistically [i.e., as $1/(\mathrm{SD})^2$]. This test is model independent, except for assumption of the Rayleigh-Ritz combination principle. The results of the consistency test are shown in Table V. The values of χ^2 returned by the fit indicate that the assigned experimental uncertainties are typically somewhat too small, suggesting the presence of small undiscovered systematic errors. However, even in the worst case ($n = 11$), there is a 6% probability of such a χ^2 arising by chance. There is, therefore, only marginal internal inconsistency in the data.

TABLE V. Test of internal consistency in experimental data set of Table IV. To perform these calculations, measurements having uncertainties greater than ±5 MHz were excluded, leaving 96 microwave-optical and three other results. Small inconsistencies are present, as indicated by the last column.

Principal quantum number	Reduced χ^2	Degrees of freedom	rms fit error (MHz)	Probability of exceeding χ^2 by chance
7	1.47	10	0.554	0.15
8	1.72	8	0.329	0.09
9	1.19	12	0.175	0.29
10	1.92	7	0.282	0.07
11	1.97	7	0.352	0.06
Weighted averages	1.59		0.361	

C. Global fitting formula

In the past, we have presented empirical fitting formulas useful for scaling transition frequencies from one principal quantum number n to another. The mass of new data has enabled us to take a more general approach. We modeled each energy level with the formula

$$E(n,L,S,J)=\frac{A(L,S,J)}{n^3}+\frac{B(L,S,J)}{n^5}+\frac{C(L,S,J)}{n^7}\,. \tag{3}$$

$E(n,L,S,J)$ represents in frequency units the displacement of an energy level from an energy reference level, which is defined below. A transition frequency ν is given by the difference between two levels, $E(n,L,S,J)-E(n,L',S',J')$. The parameters A,B,C for each (L,S,J) combination were least-squares adjusted to achieve the best fit to the measured intervals in Table IV.

In order to achieve convergence and greatest numerical stability of the fitted model, certain additional steps were necessary. First, since the data set contains no transitions between states of different n, it could provide little information about total binding energies of states. Consequently, we arbitrarily chose the $^3G_5$ state in each n manifold to be the energy reference level, and defined its energy as zero. Second, in trial fits we discovered that the n^{-7} coefficients were not significant for predominantly relativistic fine-structure intervals in F and G states, although they were for ^3D-state predominantly relativistic intervals and for all predominantly electrostatic intervals. Accordingly, for the final global fit we used a set of linear combinations of equations of the form of Eq. (3), arranged so that predominantly electrostatic and predominantly relativistic intervals were parametrized separately, as the entries in Table VI indicate. This allowed us to drop insignificant coefficients, which improved the reliability of the global fit for extrapolating to states of lower n than are covered by the data set.

In order to obtain our final results, the fitting

TABLE VI. Constants for the global fitting formula, Eq. (3) in the text, in MHz. The parameters of the fit are highly correlated. Uncertainties in the parameters are therefore given to many significant figures, in order to allow accurate calculation of the uncertainty in the predictions of the fit.

Term	A	B	C
$^1D_2$	−13 070 332.211 ± 564.283	14 956 300.794 ± 41 758.534	1 076 933.327 ± 929 858.735
$^3D_2$	−18 186 597.300 ± 717.368	36 139 902.955 ± 76 190.523	5 458 342.286 ± 2 249 058.031
$^1F_3$	−2 061 549.947 ± 586.126	5 983 700.248 ± 46 432.834	−1 513 935.770 ± 1 064 358.134
$^3D_1-{}^3D_2$	35 311.872 ± 82.981	1 700.690 ± 2 542.371	23 301.658 ± 17 134.521
$^3D_3-{}^3D_2$	−2 615.772 ± 69.448	3 796.529 ± 2 156.878	13 118.936 ± 14 456.981
$^3F_2-{}^1F_3$	−29 215.052 ± 256.303	246 543.320 ± 17 544.631	···
$^3F_3$	−54 096.898 ± 93.360	186 298.384 ± 4 466.999	···
$^3F_4$	−45 632.384 ± 275.237	236 853.260 ± 18 789.880	···
$^1G_4$	15 606.029 ± 543.873	12 571.811 ± 28 888.346	···
$^3G_3$	9 237.973 ± 562.977	13 708.161 ± 29 941.895	···
$^3G_4$	−10 768.099 ± 531.228	23 180.170 ± 28 370.848	···
$^3G_5$	0.0 [a]	0.0 [a]	···

[a] Reference level.

TABLE VII. Correlation matrix for parameters listed in Table VI. The matrix is symmetric. Rows of more than eleven elements are continued to successive lines, as are the column headings.

		$^1D_2$(A)	(B)	(C)	$^3D_2$(A)	(B)	(C)	$^1F_3$(A)	(B)	(C)	$^3D_1-{}^3D_2$(A)	(B)
		$^3D_1-{}^3D_2$(C)	$^3D_3-{}^3D_2$(A)	(B)	(C)	$^3F_2-{}^1F_3$(A)	(B)	$^3F_3-{}^1F_3$(A)	(B)	$^3F_4-{}^1F_3$(A)	(B)	$^1G_4$(A)
		$^1G_4$(B)	$^3G_3$(A)	(B)	$^3G_4$(A)	(B)						
$^1D_2$	(A)	1.000 000 0										
	(B)	−0.909 704 3	1.000 000 0									
	(C)	0.447 303 8	−0.761 206 7	1.000 000 0								
$^3D_2$	(A)	0.750 525 6	−0.689 380 6	0.318 822 2	1.000 000 0							
	(B)	−0.502 892 3	0.567 174 5	−0.401 581 8	−0.916 395 3	1.000 000 0						
	(C)	0.239 053 3	−0.389 610 0	0.424 352 6	0.739 284 6	−0.943 896 0	1.000 000 0					
$^1F_3$	(A)	0.923 267 2	−0.833 294 2	0.401 644 8	0.830 551 2	−0.620 196 5	0.373 908 1	1.000 000 0				
	(B)	−0.773 465 4	0.844 520 3	−0.640 281 6	−0.780 615 8	0.711 514 0	−0.563 066 5	−0.909 483 0	1.000 000 0			
	(C)	0.344 344 2	−0.601 153 3	0.813 234 4	0.451 619 1	−0.567 506 8	0.599 415 8	0.519 278 3	−0.814 080 6	1.000 000 0		
$^3D_1-{}^3D_2$	(A)	−0.007 043 4	0.006 736 8	−0.001 574 3	−0.021 443 5	0.022 635 1	−0.020 874 5	−0.008 595 8	0.008 957 0	−0.004 615 2	1.000 000 0	
	(B)	0.012 317 5	−0.010 720 4	0.001 828 8	0.025 544 9	−0.022 368 4	0.016 569 7	0.013 516 5	−0.012 384 9	0.004 689 3	−0.921 272 3	1.000 000 0
	(C)	−0.013 775 4	0.011 748 6	−0.001 833 8	−0.025 833 8	0.021 080 0	−0.013 969 4	−0.014 768 0	0.013 098 9	−0.004 466 4	0.841 395 0	−0.983 014 5
		1.000 000 0										
$^3D_3-{}^3D_2$	(A)	−0.064 406 2	0.026 895 0	−0.013 347 7	−0.019 790 5	−0.071 077 9	0.097 398 9	−0.066 348 5	0.039 933 4	−0.032 445 1	0.067 961 2	−0.154 020 2
		0.180 496 6	1.000 000 0									
	(B)	0.059 934 1	−0.028 038 2	0.011 357 7	0.025 593 7	0.052 789 6	−0.079 410 5	0.061 376 1	−0.038 301 0	0.027 144 1	−0.136 045 8	0.315 442 8
		−0.371 456 0	−0.927 280 9	1.000 000 0								
	(C)	−0.055 529 9	0.027 276 7	−0.010 064 6	−0.026 820 0	−0.043 136 0	0.068 717 5	−0.056 708 4	0.035 978 3	−0.023 834 3	0.157 557 1	−0.367 149 5
		0.435 392 3	0.857 949 7	−0.986 650 9	1.000 000 0							
$^3F_2-{}^1F_3$	(A)	−0.120 698 1	0.127 170 1	−0.082 859 2	0.146 462 1	−0.180 258 6	0.189 574 4	−0.146 753 7	0.150 242 9	−0.104 500 9	−0.007 485 7	0.004 953 0
		−0.003 508 8	−0.049 276 9	0.042 527 6	−0.037 971 3	1.000 000 0						
	(B)	0.117 838 1	−0.123 113 1	0.082 475 8	−0.160 277 9	0.207 787 9	−0.220 736 7	0.142 070 5	−0.150 321 9	0.111 161 1	0.094 581 0	−0.074 350 4
		0.062 006 6	−0.052 576 5	0.041 902 3	−0.035 790 3	−0.976 284 3	1.000 000 0					
$^3F_3-{}^1F_3$	(A)	−0.026 578 5	0.059 607 8	−0.091 143 8	−0.056 630 6	0.082 888 2	−0.089 941 1	−0.087 858 9	0.080 259 0	−0.064 234 4	−0.000 250 7	0.001 997 0
		−0.002 578 6	−0.114 402 0	0.094 354 2	−0.082 195 1	0.126 372 7	−0.049 884 1	1.000 000 0				
	(B)	0.048 144 7	−0.094 892 2	0.139 441 6	0.069 766 0	−0.095 507 4	0.102 474 7	0.115 650 3	−0.131 538 5	0.125 835 9	−0.000 017 1	−0.001 059 9
		0.001 427 0	0.074 166 5	−0.061 066 7	0.053 147 0	−0.129 828 0	0.075 781 0	−0.946 438 3	1.000 000 0			
$^3F_4-{}^1F_3$	(A)	−0.117 785 6	0.114 517 1	−0.075 910 5	0.136 581 3	−0.190 140 4	0.204 974 9	−0.140 220 7	0.135 458 4	−0.095 558 1	0.002 579 4	−0.015 829 6
		0.020 306 8	0.181 110 5	−0.162 947 3	0.148 572 0	0.347 367 9	−0.352 158 8	0.099 851 7	−0.112 740 2	1.000 000 0		
	(B)	0.105 535 7	−0.107 454 0	0.073 641 3	−0.148 118 3	0.198 766 4	−0.212 856 3	0.126 281 6	−0.130 485 9	0.097 176 6	−0.000 576 4	0.012 252 0
		−0.016 293 7	−0.120 623 7	0.111 850 0	−0.103 469 2	−0.334 664 3	0.346 960 3	−0.048 660 3	0.075 767 1	−0.980 752 5	1.000 000 0	
$^1G_4$	(A)	0.692 517 1	−0.357 000 4	−0.310 042 7	0.537 079 5	−0.217 077 4	−0.074 013 1	0.647 404 5	−0.304 037 1	−0.283 404 1	−0.006 538 8	0.011 819 3
		−0.013 305 3	−0.060 333 2	0.056 587 9	−0.052 621 0	−0.064 321 1	0.063 302 4	0.011 236 3	−0.010 110 5	−0.067 448 8	0.057 518 3	1.000 000 0
	(B)	−0.687 612 4	0.378 790 1	0.301 995 3	−0.551 097 9	0.258 510 0	0.030 057 4	−0.640 458 7	0.318 830 9	0.282 308 4	0.007 819 6	−0.013 240 7
		0.014 710 7	0.023 442 4	−0.027 332 3	0.027 703 8	0.071 026 4	−0.067 071 4	−0.008 583 6	0.008 761 4	0.063 309 3	−0.057 107 9	−0.983 470 6
		1.000 000 0										
$^3G_3$	(A)	0.718 664 7	−0.490 922 8	−0.015 641 6	0.538 628 9	−0.228 303 1	−0.053 145 7	0.686 532 2	−0.434 732 3	−0.020 472 2	0.018 361 2	−0.009 456 2
		0.005 432 8	−0.122 971 3	0.108 245 3	−0.097 624 1	−0.001 794 3	0.017 625 5	0.017 749 5	−0.013 308 3	−0.030 239 3	0.023 182 1	0.757 943 1
		−0.731 893 6	1.000 000 0									

TABLE VII. *(Continued)*

		$^1D_2$(A) $^3D_1-{}^3D_2$(C) $^1G_4$(B)	$^3D_3-{}^3D_2$(A) $^3G_3$(A)	(B)	(C)	$^3D_2$(A) (C) $^3G_4$(A)	(B) $^3F_2-{}^1F_3$(A) (B)	(C)	$^1F_3$(A) $^3F_3-{}^1F_3$(A)	(B) (B)	$^3F_4-{}^1F_3$(A)	(C)	$^3D_1-{}^3D_2$(A) (B)	(B) $^1G_4$(A)
$^3G_3$	(B)	−0.695 510 1	0.490 876 3	0.015 323 9	−0.524 786 9	0.237 002 9	0.042 860 5	−0.664 408 8	0.434 304 2	0.020 871 5	0.016 847 8	−0.018 354 7		
		0.017 867 2	0.059 594 7	−0.056 646 0	0.052 998 6	0.004 208 1	−0.009 592 1	−0.009 631 0	0.007 913 6	0.017 719 2	−0.014 693 0	−0.733 444 7		
		0.731 171 4	−0.979 959 3	1.000 000 0										
$^3G_4$	(A)	0.835 342 3	−0.595 955 6	0.004 780 1	0.640 560 0	−0.337 799 8	0.046 612 0	0.780 642 6	−0.512 135 0	−0.015 882 5	−0.006 089 2	0.011 191 7		
		−0.012 641 3	−0.052 141 2	0.049 660 2	−0.046 502 5	−0.070 725 3	0.069 762 8	0.013 254 4	−0.013 004 4	−0.071 173 1	0.062 571 8	0.864 761 5		
		−0.855 118 5	0.769 848 9	−0.745 733 5	1.000 000 0									
	(B)	−0.830 213 3	0.621 545 9	−0.020 114 9	−0.655 598 0	0.383 436 7	−0.096 686 2	−0.773 229 8	0.529 993 9	0.008 772 3	0.007 483 8	−0.012 729 3		
		0.014 157 6	0.015 117 1	−0.020 324 0	0.021 529 4	0.078 193 5	−0.074 298 9	−0.010 914 3	0.012 045 6	0.067 545 5	−0.062 720 8	−0.849 624 3		
		0.871 694 4	−0.739 011 7	0.739 201 9	−0.982 146 4	1.000 000 0								

program was run twice. In the first case, the input data set consisted of only the microwave-optical data, before the residual static Stark corrections had been applied (Sec. IV C above). A Stark term was included with the square of the electric field as a floating parameter, so that an estimate of the static electric field could be obtained. In the second and final case, the input data consisted of the experimental frequencies listed in Table IV. No Stark term was included in this fit. Transition frequencies calculated from the results of the final fit are listed in the third column of Table IV. Optimized values of parameters returned by the fitting program are listed in Table VI.

The reduced χ^2 of the fit (112 degrees of freedom) is 3.62, which indicates possible remaining systematic errors or deficiencies in the model, since correctly estimated random uncertainties for the data and a perfectly correct model would give a reduced χ^2 of 1. We have been able partially to separate these alternatives by comparing the model-independent fit results of Table V with model-dependent fit results.

We first ran the global fit program with the input data set restricted to only the MO data (105 values) listed in Table IV. The reduced χ^2 was 2.33 (78 degrees of freedom). By comparison, the model-independent mean χ^2 for essentially the same data set (103 MO values, 3 other "high accuracy" values) is 1.59 (Table V). We conclude that understatement of errors in the MO data contributes an excess χ^2 of about 0.59, and model error an additional 0.74, for the quantum numbers covered.

We could not perform a model-independent fit using the non-MO data alone, because it is not extensive enough. However, transition-by-transition comparison of data obtained by the various other groups, using different methods, reveals significantly greater discrepancies than for the MO results. In addition we note that the model error, if interpreted as reflecting absent higher-order terms in the formula, will increase as n decreases, and therefore should be greater for the states having only non-MO measurements, since their n values are typically lower. Evidently the larger χ^2 of 3.62 of our final model-dependent fit is increased over the MO-only value by both effects.

A theoretical basis for expressing the atomic interval as a sum in odd reciprocal powers of n has been discussed by Chang.[30] We have considered generalized versions of Eq. (3) in which the n^{-7} term was replaced by n^{-k}. Equally good fits to the experimental data were obtained for $k = 4$, 6, or 7. A modification of Eq. (3) has been proposed recently by Chang.[31] The modified formula is,

TABLE VIII. Values of $n\,^1D_2 - n\,^3D_{\text{mean}}$ intervals in ^{4}He.

n	Frequency (MHz) [a]	Other results [b]	
3	100 083 ± 694	102 130 ± 200 [c]	(E)
		120 063 [h]	(T)
		104 296 [i]	(T)
		102 339 [j]	(E)
4	58 893 ± 71	59 050 ± 80 [c]	(E)
		59 139 [j]	(E)
		66 446 [i]	(T)
		71 051 [h]	(T)
5	34 047.7 ± 10.0	34 078 ± 45 [c]	(E)
		34 066.3 ± 7.2 [d]	(E)
		34 381 [j]	(E)
		41 448 [h]	(T)
6	20 919.177 ± 1.498	20 916 ± 21 [e]	(E)
		20 918.0 ± 9.2 [d]	(E)
		20 923 ± 30 [c]	(E)
		25 657 [h]	(T)
		20 790 [j]	(E)
7	13 633.331 ± 0.196	13 629 ± 28 [e]	(E)
		13 632.8 ± 5.3 [d]	(E)
		16 776 [h]	(T)
		14 774 [j]	(E)
8	9 332.665 ± 0.080	9 326 ± 35 [f]	(E)
		9 334 ± 35 [e]	(E)
		10 800 [j]	(E)
9	6 650.483 ± 0.065	6 644 ± 35 [f]	(E)
		7 200 [j]	(E)
10	4 898.127 ± 0.073	4 889 ± 30 [f]	(E)
		5 700 [j]	(E)
11	3 707.765 ± 0.083	3 696 ± 30 [f]	(E)
		4 500 [j]	(E)
12	2 872.158 ± 0.086	2 862 ± 15 [g]	(E)
		3 900 [j]	(E)
13	2 268.962 ± 0.084	2 258 ± 15 [g]	(E)
		300 [j]	(E)
14	1 822.966 ± 0.079	1 812 ± 15 [g]	(E)
		1 800 [j]	(E)
15	1 486.275 ± 0.072	1 475 ± 20 [g]	(E)
		1 500 [j]	(E)
16	1 227.441 ± 0.065	1 215 ± 20 [g]	(E)
		300 [j]	(E)
17	1 025.252 ± 0.059	1 013 ± 20 [g]	(E)
		1 200 [j]	(E)
18	865.054 ± 0.052	852 ± 30 [g]	(E)
		2 100 [j]	(E)
19	736.507 ± 0.047	707 ± 40 [g]	(E)
20	632.179 ± 0.042	596 ± 50 [g]	(E)

[a] Present work. Values calculated from Eq. (5) in the text, based on the global least-squares fit to the experimental data in Table IV. Uncertainties are one standard deviation.

[b] E, experimental; T, theoretical.

[c] Derouard *et al.*, Ref. 34.

[d] Beyer and Kollath, Ref. 26.

[e] Miller *et al.*, Refs. 32, 33.

[f] Beyer and Kollath, Ref. 35.

[g] Beyer and Kollath, Ref. 36.

[h] Temkin and Silver, Ref. 37. We have used their polarized orbital values for the singlet states and the extended polarization values for the triplet states.

TABLE VIII. *(Continued)*

[i] Blanchard, Ref. 38.

[j] Optical data, Martin, Ref. 39.

however, much less successful than Eq. (3), as we found by fitting it to the experimental data: The reduced χ^2 for that fit is 17.74 (112 degrees of freedom).

The fitted parameters in Table VI are highly correlated. Therefore, the uncertainty of a transition frequency calculated from them must be obtained from the parameter uncertainties δA_i with the aid of the correlation matrix $\{M_{ij}\}$, which is listed in Table VII. The matrix is symmetric, and contains 351 independent elements (diagonal elements are 1 by definition). The transition frequency ν is obtained by adding or subtracting intervals calculated from the coefficients listed in Table VI. In some cases, several intervals need be combined. The uncertainty $\delta\nu$ in the transition frequency ν is calculated from the relation

$$\delta\nu = \left(\sum_{ij} \delta A_i \frac{\partial \nu}{\partial A_i} M_{ij} \frac{\partial \nu}{\partial A_j} \delta A_j \right)^{1/2} . \tag{4}$$

The quantity $\partial\nu/\partial A_i$ equals $(\pm) n^{-k}$, where $k = 3$, 5, or 7, according as A_i is a parameter A or B or C. If the term interval is added (subtracted) into ν the derivative sign is chosen positive (negative). The indices i and j run over all coefficients affecting the value of ν.

D. Comparison with low-precision data

1. Singlet-triplet D-state splittings

Singlet-triplet splittings in nD states have been measured using the magnetic-field-induced anticrossing technique by Miller and co-workers[32-34] for $n = 3$ to 8, and by Beyer and Kollath[35,36] for $n = 8$ to 20. The latter group has also used a small electric field in addition to the magnetic field, in order to measure singlet-triplet splittings in nD

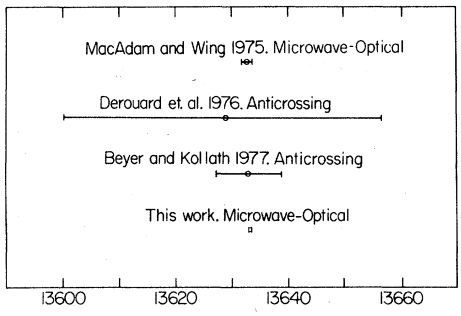

FIG. 4. Measurement of the $7\,^1D_2$-$7\,^3D_{\text{mean}}$ interval by two experimental techniques.

TABLE IX. Values of mean electrostatic fine-structure intervals in ^{4}He.

Interval	n	Frequency (MHz) [a]	Other results (MHz) [b]
$n\,^1D_2 - nF_{\text{mean}}$	4	162 733 ±19	159 310 [e] (T)
			155 000 [f] (T)
	5	84 951.95 ± 2.48	83 510 [e] (T)
			79 800 [f] (T)
	6	49 670.217 ± 0.498	48 890 [e] (T)
			46 000 [f] (T)
	7	31 471.087 ± 0.174	30 990 [e] (T)
			30 000 [f] (T)
	8	21 166.307 ± 0.074	20 840 [e] (T)
	9	14 905.712 ± 0.055	14 967 ± 160 [d] (E)
			14 680 [e] (T)
	10	10 887.056 ± 0.060	10 945 ± 120 [d] (E)
			10 720 [e] (T)
	11	8 191.150 ± 0.061	8 064 [e] (T)
	12	6 316.028 ± 0.059	
$n\,^3D_{\text{mean}} - nF_{\text{mean}}$	4	221 626 ±67	218 080 [e] (T)
			230 000 [f] (T)
	5	118 999.7 ±10.0	117 380 [e] (T)
			121 000 [f] (T)
	6	70 589.395 ± 1.648	69 710 [e] (T)
			72 000 [f] (T)
	7	45 104.418 ± 0.239	46 000 [f] (T)
			44 550 [e] (T)
	8	30 498.972 ± 0.044	30 120 [e] (T)
	9	21 556.195 ± 0.037	21 290 [e] (T)
	10	15 785.183 ± 0.042	15 590 [e] (T)
	11	11 898.915 ± 0.050	11 750 [e] (T)
	12	9 188.186 ± 0.055	
$nD_{\text{mean}} - nF_{\text{mean}}$	4	167 284 ±38	144 661 [c] (T)
	5	89 218.8 ± 5.7	74 314 [c] (T)
	6	52 744.167 ± 0.984	43 045 [c] (T)
	7	33 635.628 ± 0.168	27 121 [c] (T)
	8	22 715.613 ± 0.041	18 174 [c] (T)
	9	16 041.547 ± 0.030	12 796 [c] (T)
	10	11 739.930 ± 0.033	
	11	8 845.730 ± 0.036	
$n\,^1D - nG_{\text{mean}}$	7	37 224.185 ± 0.143	37 163 ± 60 [d] (E)
	8	25 077.274 ± 0.090	25 084 ± 30 [d] (E)
	9	17 679.933 ± 0.097	17 691 ± 65 [d] (E)
	10	12 923.783 ± 0.102	12 930 ± 60 [d] (E)
	11	9 729.342 ± 0.099	
$n\,^3D - nG_{\text{mean}}$	7	50 857.517 ± 0.134	50 812 ± 20 [d] (E)
	8	34 409.938 ± 0.102	34 397 ± 40 [d] (E)
	9	24 330.416 ± 0.093	24 368 ± 55 [d] (E)
	10	17 821.910 ± 0.102	17 819 ± 67 [d] (E)
	11	13 437.107 ± 0.111	
$nF_{\text{mean}} - nG_{\text{mean}}$	5	14 838.67 ± 4.45	14 536 [c] (T)
	6	8 928.748 ± 0.747	8 743 [c] (T)
			8 742 [e] (T)
	7	5 753.098 ± 0.209	5 628 [c] (T)
			5 620 [e] (T)
	8	3 910.967 ± 0.100	3 822 [c] (T)
			3 859 [e] (T)
	9	2 774.221 ± 0.093	2 980 [c] (T)
			2739 [e] (T)
			2 724 ± 173 [d] (E)
	10	2 036.728 ± 0.101	1 985 ± 134 [d] (E)
			2 010 [e] (T)
	11	1 538.192 ± 0.101	1 518 [e] (T)

TABLE IX. *(Continued)*

[a] Present work. Values calculated from global least-squares-fit results. Uncertainties are one standard deviation.
[b] E, experimental; T, theoretical.
[c] Deutsch, Ref. 18.
[d] Beyer and Kollath, Ref. 10.
[e] Chang and Poe, Ref. 20.
[f] Temkin and Silver, Ref. 37.

($n=5$ to 7).[26] Anticrossing is inherently a lower-precision technique than the MO technique because the high magnetic field produces a motional Stark effect, which can easily broaden the resonances by two orders of magnitude and shift the resonance position drastically. The shift can be calculated approximately using hydrogenic wave functions,[10] but the fine-structure sublevels are almost always unresolved. The effect is particularly severe in a light atom because of its high thermal speed. Consequently, only one anticrossing study[26] has succeeded in resolving an interval in the $n\,^3D_J$ multiplet; all the other studies measured the $n\,^1D_2$-$n\,^3D_{\rm mean}$ splitting.

In Table VIII we compare the anticrossing measurements with the values returned by the global fit to our measurements, using a statistical weight of $2J+1$ for each ^3D_J level to calculate the ^3D mean energy. These anticrossing data were excluded from the input to the global least-squares fit. Theoretical estimates[37,38] and optical spectroscopic data[39] are also included in the table. Intervals for n greater than 20 are not shown in the table but can be computed using the global fitting formula (3). Substituting the constants from Table VI and performing the average over ^3D_J, we obtain

$$\nu(n\,^1D_2-n\,^3D_{\rm mean}) = \frac{5\,110\,423.4}{n^3}-\frac{21\,185\,714.13}{n^5} - \frac{4\,391\,991.6}{n^7}\ \text{MHz}. \quad (5)$$

The uncertainty approaches 100 ppm for high n.

The anticrossing results are consistent with the values returned by the global least-squares fit and have an uncertainty typically two orders of magnitude larger, except in $n=3$ to 5. Indeed, the uncertainties returned by the anticrossing technique are typically larger than the smallest interval among the ^3D levels. Figure 4 displays the results of two anticrossing measurements and two MO measurements for the $7\,^1D_2$-$7\,^3D_{\rm mean}$ interval. The two MO measurements are consistent and have much smaller error bars than the anticrossing measurements. Not shown are the results of optical measurements; typical error bars are 300 MHz.

2. *Mean D-F-G splittings*

Beyer and Kollath[10] have used the technique of electric-field-induced anticrossing to measure intervals from $n\,^1D_2$ or $n\,^3D_{\rm mean}$ to $nF_{\rm mean}$ and $nG_{\rm mean}$. Their experiments did not resolve the individual F or G sublevels. In Table IX we compare these measurements with the results of the global fit to the data in Table IV. We have weighted each $^{1,3}L_J$ level by its statistical weight $2J+1$ in calculating the average energy for a group of levels. These anticrossing data were not included in the input data for the global least-squares fit. They are in agreement with it, but are typically two orders of magnitude less precise.

Also shown in Table IX are theoretical estimates by Temkin and Silver[37] and by Deutsch,[18] based on polarization theory; and by Chang and Poe,[19,20] based on a Brueckner-Goldstone many-body approach. The inaccuracy of present theory for electrostatic fine structure in helium is apparent.

VII. CONCLUSION

With the completion of this measurement series, we feel we have reached a turning point in the spectroscopy of atomic helium. In this and our earlier papers, we have presented sub-MHz results for most transitions that lie in the approximate range 7 to 50 GHz. At the level of precision of a few MHz, the poorly charted territory that remains consists of transitions to states whose angular momentum L exceeds 4; a few D-F-G transitions in states having $n<6$; transitions involving S and P terms, including those in which n changes; and the ^{3}He isotope. Measurements with worse than a few MHz precision of ^{4}He D-F-G transitions for $n>11$ are *not* needed, since the global fit results model these accurately. The reliability of the global fitting formula should improve with n, because in the asymptotic regime the n^{-3} term dominates. The formula then predicts a constant quantum defect, a well-known result in atomic spectroscopy.

In this article we have demonstrated the superiority of the microwave-optical technique as a spectroscopic tool for Rydberg states. Similarly, it is apparent that the microwave-optical method

of ^{4}He Rydberg-state spectroscopy, in its implementation in our laboratory, has put itself largely out of business by its own success. Most further progress will require substantial modifications in excitation, resonant transition, and detection methods, including the use of high-resolution, accurately calibrated laser sources. We are pursuing some of these alternatives at present.

In the realm of theory, nearly the whole helium energy-level spectrum is unexplored at the MHz level of accuracy. In view of helium's unique role as the simplest multielectron atom, and as a natural example of the quantal three-body problem, renewed theoretical interest in the topic is desirable.

ACKNOWLEDGMENTS

This work was supported in part by NSF Grant No. PHY77-15217. One of us (K.B.M.) held an NSF energy-related postdoctoral fellowship, and one of us (J.W.F.) held an NSF national needs postdoctoral fellowship, during part of this research. We would like to thank August H. Johnson for much help in the automation of the apparatus.

---

*Present address: Dept. of Physics and Astronomy, Univ. of Kentucky, Lexington, Ky. 40506.

[1]W. H. Wing and W. E. Lamb, Jr., Phys. Rev. Lett. 28, 265 (1972).

[2]W. E. Lamb, Jr., D. L. Mader, and W.H. Wing, in *Fundamental and Applied Laser Physics, Proceedings of the Esfahan Symposium*, edited by M. S. Feld, A. Javan, and N. A. Kurnit (Wiley, New York, 1973), pp. 523–538; W.H.Wing, K. R. Lea, and W. E. Lamb, Jr., in *Atomic Physics 3*, edited by S. J. Smith and G. K. Walters (Plenum, New York, 1973), pp. 119–141.

[3]W. H. Wing and K. B. MacAdam, in *Progress in Atomic Spectroscopy*, edited by W. Hanle and H. Kleinpoppen (Plenum, New York, 1978), pp. 491–527.

[4]K. B. MacAdam and W. H. Wing, Phys. Rev. A 12, 1464 (1975), referred to in the text as I.

[5]K. B. MacAdam and W. H. Wing, Phys. Rev. A 13, 2163 (1976), referred to in the text as II.

[6]K. B. MacAdam and W. H. Wing, Phys. Rev. A 15, 678 (1977), referred to in the text as III.

[7]G. Astner, L. J. Curtis, L. Liljeby, S. Mannervik, and I. Martinson, J. Phys. B 9, L345 (1976).

[8]R. K. Van den Eynde, G. Wiebes, and Th. Niemeyer, Physica (Utrecht) 59, 401 (1972).

[9]A. C. Tam, J. Phys. B 9, L559 (1976).

[10]H. J. Beyer and K. J. Kollath, J. Phys. B 11, 979 (1978).

[11]M. Rosenbluh, A. Panock, B. Lax, and T. A. Miller, Phys. Rev. A 18, 1103 (1978).

[12]R. Panock, M. Rosenbluh, B. Lax, and T. A. Miller, Phys. Rev. Lett. 42, 172 (1979).

[13]J. W. Farley, A.H. Johnson, and W. H. Wing (unpublished).

[14]T. F. Gallagher and W. E. Cooke, Phys. Rev. Lett. 42, 835 (1979); E. J. Beiting, G. F. Hildebrandt, F. G. Kellert, G. W. Foltz, K. A. Smith, F. B. Dunning, and R. F. Stebbings, J. Chem. Phys. 70, 3551 (1979).

[15]J. W. Farley and W. H. Wing (unpublished).

[16]A. H. Gabriel and D. W. O. Heddle, Proc. R. Soc. London A 258, 124 (1960).

[17]H. Bethe and E. Salpeter, *Quantum Mechanics of One- and Two-Electron Atoms* (Springer, Berlin, 1957).

[18]C. Deutsch, Phys. Rev. A 13, 2311 (1976).

[19]T. N. Chang and R. T. Poe, Phys. Rev. A 14, 11 (1976).

[20]T. N. Chang and R. T. Poe, Phys. Rev. A 10, 1981 (1974).

[21]A. C. Tam, Phys. Rev. A 12, 539 (1975).

[22]J. P. Descoubes, in *Physics of One- and Two-Electron Atoms*, edited by F. Bopp and H. Kleinpoppen (North-Holland, Amsterdam, 1969), pp. 341–347.

[23]H. G. Berry, J. L. Subtil, and M. Carre, J. Phys. (Paris) 33, 947 (1972).

[24]N. Bessis, H. Lefebvre-Brion, and C. M. Moser, Phys. Rev. 135, A957 (1964).

[25]R. M. Parish and R. W. Mires, Phys. Rev. A 4, 2145 (1971).

[26]H. J. Beyer and K. J. Kollath, J. Phys. B 10, L5 (1977).

[27]R. D. Kaul, J. Opt. Soc. Am. 58, 429 (1968).

[28]J. Brochard, R. Chabbal, H. Chantrel, and P. Jacquinot, J. Phys. Radium 18, 596 (1957).

[29]D. Dily and J. P. Descoubes, C. R. Acad. Sci. Paris B 272, 1182 (1971).

[30]T. N. Chang, J. Phys. B 7, L108 (1974).

[31]T. N. Chang, J. Phys. B 11, L583 (1978).

[32]T. A. Miller, R. S. Freund, F. Tsai, T. J. Cook, and B. R. Zegarski, Phys. Rev. A 9, 2474 (1974).

[33]T. A. Miller, R. S. Freund, and B. R. Zegarski, Phys. Rev. A 11, 753 (1975).

[34]J. Derouard, R. Jost, M. Lombardi, T. A. Miller, and R. S. Freund, Phys. Rev. A 14, 1025 (1976).

[35]H. J. Beyer and K. J. Kollath, J. Phys. B 8, L326 (1975).

[36]H. J. Beyer and K. J. Kollath, J. Phys. B 9, L185 (1976).

[37]A. Temkin and A. Silver, Phys. Rev. A 10, 1439 (1974).

[38]P. Blanchard and G. W. F. Drake, J. Phys. B 6, 2495 (1973).

[39]W. C. Martin, J. Phys. Chem. Ref. Data 2, 257 (1973).